Available online at www.sciencedirect.com

ScienceDirect

Proceedings of the Combustion Institute 38 (2021) 6503–6511

Proceedings of the Combustion Institute

www.elsevier.com/locate/proci

Flame spray pyrolysis made Pt/TiO_2 photocatalysts with ultralow platinum loading and high hydrogen production activity

Fuchang Gao [a,b], Zuwei Xu [a,b,*], Haibo Zhao [a,b,*]

[a] *State Key Laboratory of Coal Combustion, School of Energy and Power Engineering, Huazhong University of Science and Technology, 1037 Luoyu Road, Wuhan 430074, PR China*

[b] *China-EU Institute for Clean and Renewable Energy, Huazhong University of Science and Technology, Wuhan 430074, PR China*

Received 8 November 2019; accepted 28 June 2020
Available online 9 September 2020

Abstract

In this paper, flame spray pyrolysis (FSP) is used to synthesize Pt/TiO_2 catalysts with surface-supported isolated Pt atoms through elaborate precursor/solvent formulation and flame temperature history control. It is a pivotal factor to this FSP process that there is a major distinction on saturated vapor pressure between two components (Pt species and Ti species), and thereby they exist as gas phase and particle phase at a certain temperature range, respectively. When the flame is quenched to ambient temperature with cold sheath gas, Pt species of gaseous PtO_2 (being in the vapor phase above 723 K) condense into deposition state on the surface of TiO_2 nanoparticles. Combined with X-ray photoelectron spectroscopy (XPS) analysis and high-angle annular dark-field scanning transmission electron microscopy (HAADF-STEM) detection, we identify that Pt atoms are dispersed and anchored on the catalyst surface. Single-atom Pt dispersed Pt/TiO_2 catalysts can be well achieved by controlling the loading at a very low level, which offers an effective way to maximize the atom economy for surface catalysis of scarce noble metals. In this work, considering that Pt as the best co-catalyst of hydrogen evolution, the FSP-made Pt/TiO_2 catalysts are tested in a photocatalysis water splitting system aiming to a simple and attractive means of renewable hydrogen production. The highest activity presents in $0.1Pt/TiO_2$ with 0.1% molar ratio of Pt to Ti, reaching 108.5 times of the benchmark sample from commercial flame-made TiO_2 (P25). The high activity is attributed to the fact that the isolated Pt atom serves as the main active site for photocatalysis hydrogen evolution. Therefore, the performance and cost efficiency of catalysts are greatly improved by the FSP, mainly ascribed to engineering atomically dispersing Pt on the support surface.

Keywords: Flame spray pyrolysis; Nanoparticles; Platinum; Single-atom catalysis; Photocatalytic hydrogen production

* Corresponding authors at: State Key Laboratory of Coal Combustion, School of Energy and Power Engineering, Huazhong University of Science and Technology, 1037 Luoyu Road, Wuhan 430074, PR China.

E-mail addresses: xuzw@hust.edu.cn (Z. Xu), hzhao@mail.hust.edu.cn (H. Zhao).

https://doi.org/10.1016/j.proci.2020.06.330

1. Introduction

Hydrogen has been considered as the most promising of all the energy carriers because it could provide a clean sustainable energy route without the exhaust emissions that arise from the combustion of fossil or biomass fuels [1]. Among the various technologies available, photocatalytic water splitting shows an enduring attraction as a simple means of renewable hydrogen production harnessing natural sunlight and water, viable for long time to come [2]. The development of particulate photocatalysts driving water splitting efficiently has a significant impact because such systems can be spread on a large scale using inexpensive particle-water mixtures [3]. However, there are still many challenges in improving the energy conversion efficiency, such as extending the wavelength range of absorption photons, enhancing the reaction activity for hydrogen evolution, and reducing the cost of photocatalyst materials [4].

Flame synthesis is widely used for solving high performance and high yields of materials preparation, in which process parameters can be adjusted to produce nanoparticles with varied crystallinity and morphology without post-treatments [5–7]. Especially, flame spray pyrolysis (FSP), developed in the last decades, is a versatile technique in the family of flame synthesis because it offers in contrast to conventional flame methods more flexibilities regarding material choice and design [8,9]. A well-known example of flame synthesized TiO_2 nanoparticles is Evonik-Degussa P25, which was used as the main material or test benchmark in numerous photocatalysis studies [10]. Since the Honda–Fujishima effect was discovered in 1972, TiO_2 has continuously attracted great interest with a good application prospect because it is nontoxic, abundant, cheap and thermochemical stable [11]. However, large band gap (3.0–3.2 eV) makes TiO_2 only have a light response in the ultraviolet region of about 5% of solar energy, which limits its solar-to-hydrogen (STH) energy conversion efficiency. In order to improve the STH efficiency by increasing solar absorption, many TiO_2 modification methods have appeared, for example, metal ion doping, anion doping, semiconductor compound and so on [12].

Recently, CuO*x*/TiO_2 photocatalysts were prepared by a FSP method in our group, in which lattice doping and nanocluster modification of Cu species on a TiO_2 substrate were simultaneously controlled during the FSP process to promote charges separation and induce visible-light absorption [13]. Although the H_2 production rate of the optimal sample consisting of 2 mol% Cu was *ca.* 22.1 times higher than that of the commercial P25 TiO_2, it still remains less than the samples loaded with noble metal Pt. As is well known, Pt is the most efficient co-catalyst in photocatalytic hydrogen evolution for H^+ reduction and the combination of surface hydrogen atoms into molecular H_2 [14], but its high cost limits its wide application. Therefore, it is desirable to develop photocatalysts that only need minimal amounts of Pt to function and still possess high activity.

Downsizing noble metals from particles to clusters or even single atoms offers an effective way to maximize the atom utilization. Single-atom catalysts (SACs) with atomically dispersed noble metal loaded on substrates have attracted increasing research interests, which provides the maximum atom economy and ideal cost efficiency as well as results in superior catalytic activity and/or high selectivity [15]. Xing et al. [16] identified that isolated Pt atoms are active sites for hydrogen evolution in the configuration of Pt/TiO_2 photocatalysts. Li et al. [17] reported that the single-atom Pt as co-catalyst anchored on g-C_3N_4 with high dispersion and stability, can remarkably enhance the photocatalytic H_2 evolution activity.

Although diverse preparation methods of SACs have been proposed, such as co-precipitation, co-impregnation, photochemical strategy, atomic layer deposition, these conventional chemical methods are mainly used for fundamental studies and are generally subject to low yields and time-consuming processes [18]. FSP has exhibited great potential in one-step direct synthesis of Pd subnano-clusters and even single-atoms supported on TiO_2 with superior catalytic performance [19–21]. However, large research space still remains in light of the fact that the choice of precursors, the optimization of loading, the control of flame atmosphere and high-temperature residence time are crucial for improving their atom efficiency. For instance, FSP can increase the threshold of metal loading due to surface and bulk uniform mixing of component species at the atomic level [13,22], but for SACs applications, only surface-supported atoms can effectually act as active sites in heterogeneous catalysis. Therefore, it is necessary to innovatively design and control FSP process parameters according to updated requirements.

Here we use FSP method to prepare Pt/TiO_2 catalysts with ultralow Pt loading and remarkable catalytic performance towards photocatalytic hydrogen production. The properties of the as-synthesized catalysts are researched by X-ray diffraction (XRD), X-ray photoelectron spectroscopy (XPS), aberration-corrected high-angle annular dark field scanning transmission electron microscopy (AC–HAADF-STEM), inductively coupled plasma-optical emission spectrometer (ICP-OES) and other characterization methods. Moreover, the hydrogen production activity is investigated in a photocatalytic test system. These experimental results demonstrate that atomically dispersed Pt on TiO_2 surface is

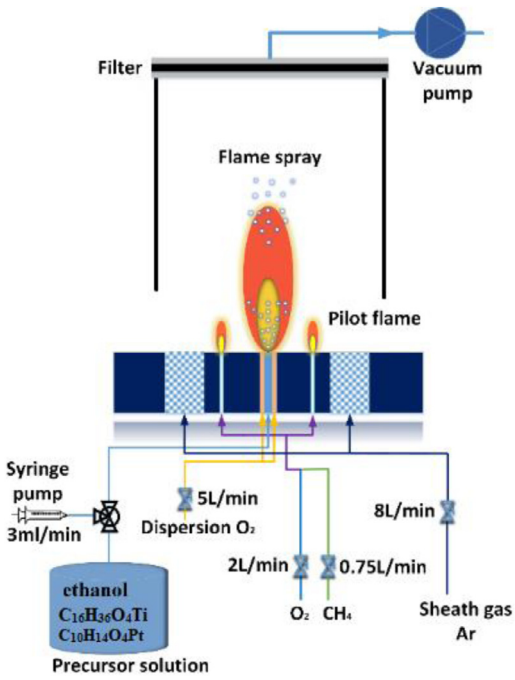

Fig. 1. Schematic view of flame spray pyrolysis system.

the most important cause of superior catalytic activity and atom efficiency. Furthermore, a possible mechanism about single-atom Pt dispersion and loading in the flame environment is illustrated.

2. Experimental

2.1. Catalyst preparation by FSP

The Pt/TiO_2 samples used in the experiments are prepared using a laboratory scale FSP system (NPS10, Tethis SpA) as shown in Fig. 1. A precursor solution consists of 90 ml absolute ethanol (C_2H_6O, Sinopharm Chemical Reagent) and 10 ml of tetrabutyl titanate ($C_{16}H_{36}O_4Ti$, Sinopharm Chemical Reagent) for all cases, and a quantity of platinum acetylacetonate ($C_{10}H_{14}O_4Pt$, Aladdin) as a Pt precursor is dissolved in the mixed solution. We adjust parameters of the FSP process and prepare seven photocatalyst samples with different Pt loading concentration from 0 to 0.5 mol% (Pt/Ti), denoted as *r*Pt/TiO_2, where *r* is the percent of atomic ratio of platinum to titanium. The detailed precursor ratio and experimental parameters are shown in Fig. 1 and Table 1.

When the FSP process starts, the precursor solution is fed at a constant flow rate into a two-fluid atomizing nozzle that uses pure oxygen as dispersion gas with high velocity to break the liquid into fine droplets. Then, the mist of small droplets is ignited by a surrounding annular pilot flame (premixed CH_4–O_2) to form a high temperature turbulent flame. The subsequent conversion of the metal salts to the metal oxides occurs upon the pyrolysis and oxidation reaction, and the metal oxide monomers further grow into nanoparticles after undergoing successive evolutions of nucleation, coagulation, sintering and so on [7]. Afterwards, the aerosol flame is quenched to ambient temperature with cold sheath gas due to turbulent entrainment. Finally, the mature nanoparticles are collected as powder by a glass-microfiber filtration system above the burner. Note that the nanoparticle production is a complicated function of the process parameters such as material concentration profile, temperature field and flow field within the high temperature environment. Nowadays, a lack of *in-situ* measurement techniques amplifies the difficulties in detailed understanding of the FSP process [5,23].

Table 1.
Pt loading and corresponding precursor dosage of all seven Pt/TiO_2 catalysts.

Sample	Pt/Ti (mol%)	$C_{10}H_{14}O_4Pt$ (mg)
$0Pt/TiO_2$	0	0
$0.025Pt/TiO_2$	0.025	3.0
$0.05Pt/TiO_2$	0.050	6.0
$0.075Pt/TiO_2$	0.075	9.0
$0.1Pt/TiO_2$	0.100	12.0
$0.2Pt/TiO_2$	0.200	24.0
$0.5Pt/TiO_2$	0.500	60.0

2.2. Photocatalytic hydrogen production activity test

Photocatalytic hydrogen production activity of the samples is tested using a water splitting H_2 production equipment (CEL-SPH2N, Beijing CEAulight) with batch gas sampling valves and an online gas chromatography (TCD detector, 99.999% high-purity N_2 as carrier gas). The experimental system consists of a 300 W Xe lamp light source (CEL-HXF300, Beijing CEAu-light), a 250 mL quartz glass reactor, a gas circulation system and a vacuum system (consisting of glass pipelines and a vacuum pump). Schematic view of the hydrogen production system is shown in Fig. S1, Supporting Materials (SM), and a detailed description of experimental system and procedures can also be found in Section S1, SM.

2.3. Instrument information of catalyst characterization

2.3.1. Structure analysis

A powder X-ray diffraction (XRD) pattern is recorded using a X-ray diffractometer (Emprean, PANalytical) (Cu Kα as the radiation source, $\lambda = 0.1542$ nm). The specific surface area

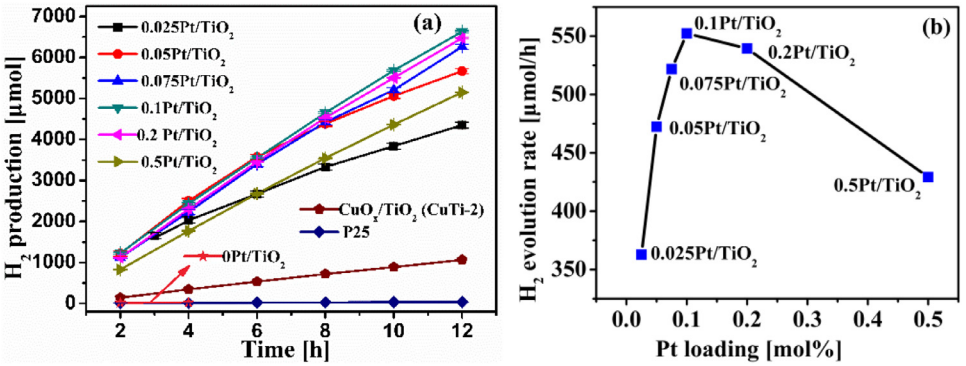

Fig. 2. Photocatalytic hydrogen production activity tests of different samples: (a) hydrogen production curve; (b) hydrogen evolution rate (12-h average).

of the sample is characterized in a physisorption apparatus (Micromeritics ASAP-2020) using the Brunauer–Emmett–Teller (BET) method. The UV–visible diffuse-reflectance spectra (UV–Vis DRS) of samples at 200–1000 nm are obtained by a UV–Vis spectrophotometer (Lambda 35, Perkin Elmer). The nanoparticle size, morphology, and crystal phase are analyzed at a field-emission transmission electron microscope (FETEM) (Talos F200X, FEI) with a resolution of 0.16 nm and an acceleration voltage of 200 kV. The occurrence state of platinum species is analyzed by a spherical aberration-corrected high-angle annular dark field scanning transmission electron microscope (AC–HAADF-STEM) (JEM-ARM200F, JEOL), with a STEM-HAADF resolution of 0.08 nm and an acceleration voltage of 200 kV.

2.3.2. Component analysis

The X-ray photoelectron spectroscopy (XPS) of the sample is tested on the X-ray photoelectron spectrometer (ESCALAB 250Xi, Thermo Fisher), setting the calibration peak position of C1s to 284.8 eV to correct the binding energy of the element. Pt loadings are determined by an inductively coupled plasma-optical emission spectrometer (ICP-OES) (ICAP 7200, Thermo Fisher). Temperature programmed desorption test of H_2 (H_2-TPD) is performed on a chemisorption analyzer (AutoChem II-2920, Micromeritics) to explore the interaction between Pt and TiO_2, and the experimental process and analysis are detailed in Section S2, SM.

3. Results and discussion

3.1. Photocatalytic hydrogen production performance

The as-synthesized samples and the benchmark sample P25 TiO_2 (Evonik–Degussa) are subjected to photocatalytic hydrogen production activity test. It can be seen from Fig. 2(a) that the activity of Pt-loaded TiO_2 is greatly improved compared with P25 and hydrogen produces steadily as a function of time. In Fig. 2(b), the hydrogen evolution rate (HER) first increases and then decreases with the increase of the loading amount. It can be noted that the sample 0.1Pt/TiO_2 has the highest photocatalytic activity, and the HER is measured to be 552.39 μmol/h, which is 107.5 times more than that of P25 (5.09 μmol/h). The activity of the FSP-synthesized pure TiO_2 (0Pt/TiO_2 with HER of ~ 5.81 μmol/h) is similar to that of P25, which verifies from the side that the loading of Pt is the important reason for the increase in activity. Movie S1 also demonstrates that many conspicuous hydrogen bubbles are readily released in the reaction solution of 0.1Pt/TiO_2. In addition, Pt/TiO_2 samples are compared with our previous CuO_x/TiO_2 samples [13]. Under the same test conditions, the HER is 112.6 μmol/h for CuTi-2 (with Cu content of 2 mol%) as the best one in CuO_x/TiO_2 catalysts, which reaches only 20.4% of 0.1Pt/TiO_2.

Table 2
Pt loading measured by ICP-OES.

Sample	Pt/Ti (mol%)		Error (%)
	Designed	Measured	
0.05Pt/TiO_2	0.050	0.059	18.0
0.1Pt/TiO_2	0.100	0.108	8.0
0.5Pt/TiO_2	0.500	0.588	17.6

Furthermore, to evaluate the photocatalytic activity stemming from Pt loading, the apparent turnover frequency (TOF) was estimated by the equation:$\mathrm{TOF} = C_{H_2}/(N_{Pt}D)$. Here the number of hydrogen turnovers C_{H_2} (mol H_2 g^{-1} h^{-1}) is calculated from the hydrogen production rate, the Pt loading N_{Pt} (mol g^{-1}) is determined from the ICP-OES measurements (the results of three typical samples are shown in Table 2), the Pt dispersion D uses the ideal dispersion assumption, $D = 1$. Note

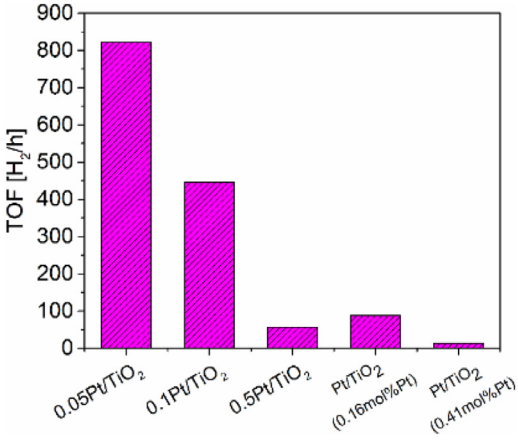

Fig. 3. TOFs of 0.05Pt/TiO_2, 0.1Pt/TiO_2, 0.5Pt/TiO_2, and compared with two Pt-loaded TiO_2 photocatalysts reported in literatures [25,26].

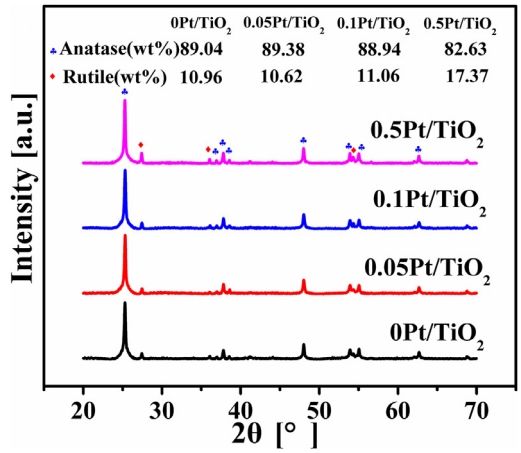

Fig. 4. XRD patterns of the samples.

that because of the extremely low Pt loading in Pt/TiO_2 samples, the metal dispersion measured by the usual chemisorption techniques are not satisfactory [24], and thereby we fail to measure the Pt dispersion and instead use the ideal dispersion to estimate the number of active sites, which actually underestimates the TOF values.

In Fig. 3, TOF varies from 822 H_2/h to 56.3 H_2/h with decrease over 93% among the three typical samples, which implies that the utilization of Pt reduces with the increase of Pt loading. We calculate the apparent TOF using ideal dispersion $D = 1$, assuming that all Pt can expose on the surface as active sites. In fact, the high Pt loading is conducive to forming large Pt clusters in which part of Pt inside the clusters cannot contribute to hydrogen evolution, thus dragging down the TOF value. Under the same test conditions, compared with two Pt/TiO_2 samples (0.16 mol% Pt and 0.41 mol% Pt loaded by photodeposition method) that are the best performing Pt/TiO_2 photocatalyst in Refs. [25,26], the TOFs of 0.1Pt/TiO_2 and 0.5Pt/TiO_2 are approximately 4 and 3 times more than them, respectively, with similar Pt loading.

To study the effect of Pt loading on the optical properties of catalysts, UV–Vis analysis is performed (details in Section S3, SM). As shown in Fig. S2a, there is no significant visible-light response almost, and the visible light absorbance is marginally enhanced when the Pt loading is 0.5 mol%. In Fig. S2b, the Pt-free TiO_2 has a band gap of about 3.20 eV, consistent with known experimental values. Other three Pt/TiO_2 samples have band gaps of 3.19 eV, 3.16 eV, and 3.07 eV, respectively. This indicates that the effect of Pt loading on the absorption of visible light is very limited, at least not an important aspect. As for previous CuOx/TiO_2 photocayalysts, we had realized that Cu species improved charge separation and extended spectral response by lattice doping and cluster modification [13]. It would be reasonable to consider that the functional principles of the two catalysts of Pt/TiO_2 and CuOx/TiO_2 are different. To understand why Pt/TiO_2 photocatalyst with ultralow Pt loading possesses higher hydrogen production activity, we perform further characterization and analysis.

3.2. Catalysts characterization

The XRD patterns show the crystal structure and phase composition of the samples with four different Pt loadings (In Fig. 4). According to the diffraction peak, most of the TiO_2 is anatase phase with mainly crystal face (101), only a small amount is rutile phase with mainly crystal face (110). No diffraction peak of Pt or Pt oxides is found potentially due to the ultra-low content of Pt and a highly dispersed state. The content ratio of anatase and rutile in the sample is calculated according to Ref. [27] (details in Section S3, SM), which is basically constant, except that the rutile content of 0.5Pt/TiO_2 increases slightly. It suggests that Pt has little effect on the crystal phase composition of TiO_2 at very low loading.

Furthermore, FETEM is used for observing the microstructure of representative samples. For 0.1Pt/TiO_2, a high resolution transmission electron microscopy (HRTEM) image (Fig. 5(a)) indicates that the particles mainly contain anatase (101) and rutile (110) with diameter in the order of 10 nm, consistent with BET specific surface area analysis (Fig. S3). AC–HAADF-STEM with sub-angstrom resolution is used to identify the nature of platinum species for two typical samples 0.1Pt/TiO_2 and 0.5Pt/TiO_2. For 0.1Pt/TiO_2, isolated heavy atom Pt with bright contrast can be discerned on the surface of TiO_2 nanocrystals (Fig. 5(b)), and correspond-

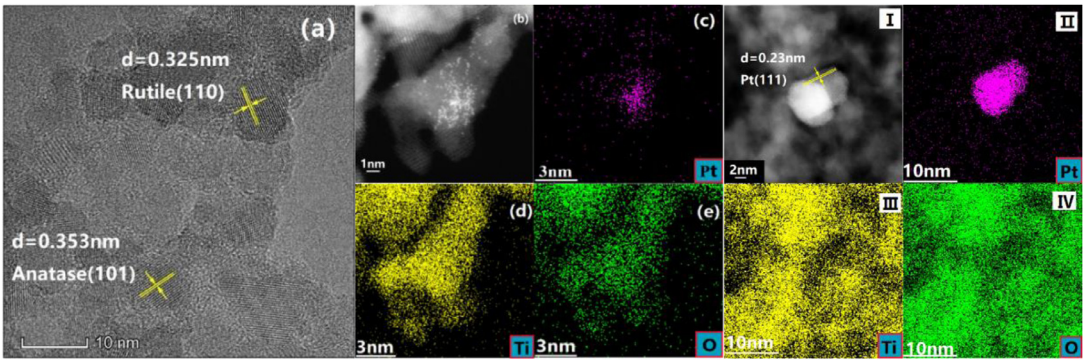

Fig. 5. Microstructure characterization of sample 0.1Pt/TiO_2 (a)–(e) and 0.5Pt/TiO_2(I)–(IV): (a) HRTEM; (b) and (I) AC–HAADF-STEM; (c)–(e) and (II)–(IV) EDS element mapping.

ing energy-dispersive X-ray spectroscopy (EDS) clearly shows the elemental mapping of Pt, Ti and O (Fig. 5(c)–(e)). Additionally, 0.5Pt/TiO_2 sample comprises both Pt single atoms and Pt nanocrystals observed in Fig. 5(I)–(IV). Therefore, it would be reasonable to think that as the Pt loading increases, the surplus Pt atoms tend to form large metal clusters covering up the dispersed Pt atoms.

XPS is used to investigate the chemical states of Pt on the surface of the catalysts. The high-resolution Pt 4f XPS spectra of samples are shown in Fig. 6. We can see that there are three chemical states of Pt element (Pt^{4+}, Pt^{2+}, Pt^0) in each sample, most in the form of high oxidation state Pt^{4+} and barely a small amount of Pt^0. Moreover, as the Pt loading increases, the proportion of Pt^{4+} reduces, but the contents of Pt^{2+} and Pt^0 increase. The presence of Pt^0 is attributed to Pt metal clusters while the oxidation state Pt is originated most probably from a strong metal-support interaction (SMSI) between Pt and the TiO_2 support [28]. Especially for single-atom Pt dispersed on TiO_2 surface, it is more conducive to forming a high oxidation state. Xing et al. [16] demonstrated through experiments and theoretical calculations that the single atomic Pt in the oxidation state on the surface of TiO_2 was the main active site of photocatalytic hydrogen evolution, while the metal Pt cluster nanoparticles on photocatalytic hydrogen production had little contribution to the activity. On the other side, the atomic ratios of Pt to Ti for the three samples are 0.46 mol%, 0.71 mol%, 2.70 mol% derived from XPS spectrum analysis (Fig. S4), respectively, which are far more than that of ICP-OES results in Table 2. Thereby, we can infer that Pt species are mainly enriched on the surface of TiO_2 nanoparticles.

The experimental results of H_2-TPD (details in Section S2) also reveal the SMSI between Pt and TiO_2 based on reverse hydrogen spillover [28]. Figure 7 shows that the desorption peak of hydrogen on the Pt-loaded TiO_2 is higher, and the desorption temperature of hydrogen is lowered. This indicates that in the adsorption process of hydrogen, the presence of Pt can promote the dissociation of H_2 and the transfer of H^+ to TiO_2, thereby increasing the adsorption amount of hydrogen; in the desorption process, the presence of Pt promotes the reverse hydrogen spillover from TiO_2 to Pt, thereby increasing the desorption amount of H_2 and lowering the desorption temperature. That is, in the photocatalytic hydrogen production reaction, H^+ can be more easily transferred to the Pt atoms, accepting photoelectrons from TiO_2 to form adsorbed H atoms, and combine each other to form hydrogen molecules and then desorb from the catalyst surface. Therefore, we can speculate that the existence of Pt promotes the separation of electron-hole pairs, but also accelerates hydrogen transfer to Pt to form hydrogen molecules due to the reverse hydrogen spillover, thereby improving the hydrogen production activity.

3.3. Single-atom Pt dispersion and loading in flame

As mentioned above, intrinsic activity improvement of Pt/TiO_2 results from isolated and efficiently-utilized Pt atoms on the surface of TiO_2 nanoparticle. Therefore, FSP offers a facile route to synthesize SACs in one step compared with other existing methods that generally involve time-consuming and expensive processes such as co-precipitation, further impregnation, drying, and annealing. Since temperature is a critical parameter for synthesis and stability of SACs, it is very important to investigate temperature history of FSP that has an unique *in-situ* calcination process. Consequently, the axial temperature is measured by a B-type (Pt/30%Rh–Pt/6%Rh) fine-wire thermocouple (details in Section S4) in pure ethanol spray flame because the combustion enthalpy of the precursor mixture was found to be reasonably similar [29,30]. The measured temperatures are corrected afterward for radiation loss according to Ref. [31].

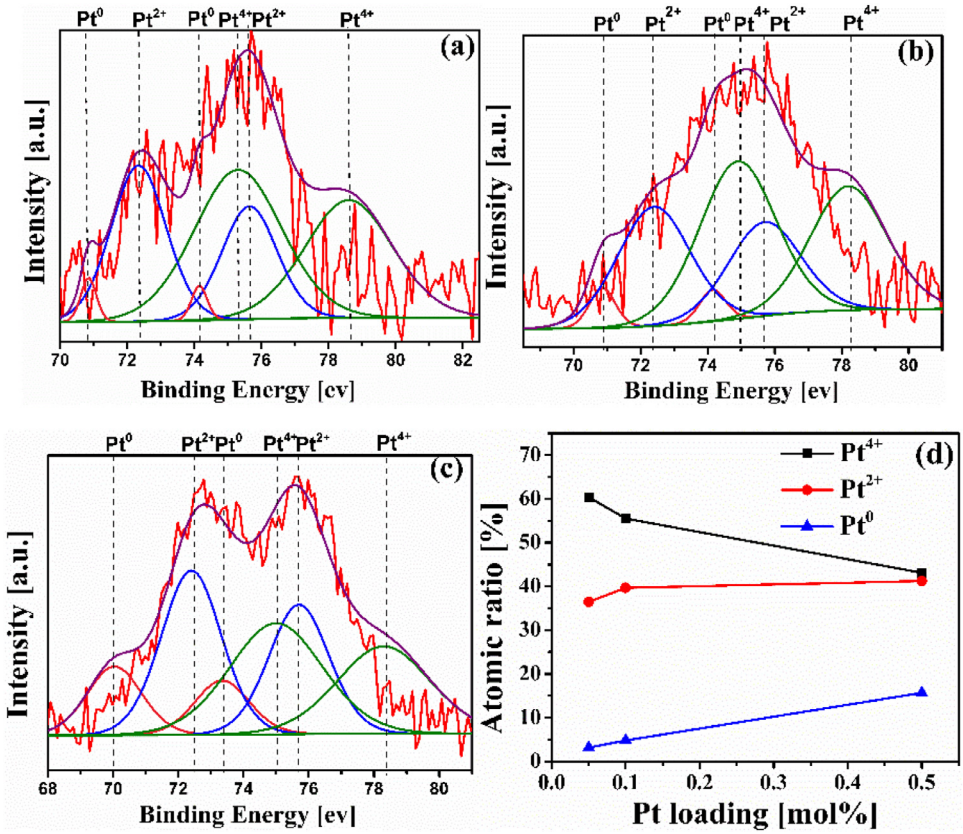

Fig. 6. XPS of Pt element in Pt/TiO_2 samples: (a) $0.05Pt/TiO_2$; (b) $0.1Pt/TiO_2$; (c) $0.5Pt/TiO_2$; (d) atomic ratio of three chemical states *vs*. Pt loading.

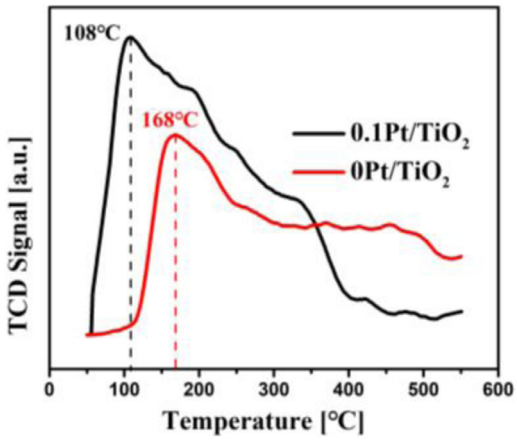

Fig. 7. H_2-TPD curves of $0.1Pt/TiO_2$ and pure TiO_2.

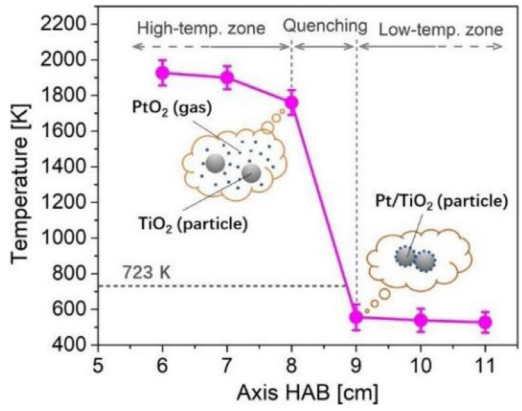

Fig. 8. Effect of temperature on the formation of surface-loaded atomically dispersed Pt/TiO_2 nanoparticles.

Note that due to excessive temperature below 6 cm height above the burner (HAB), which exceeds the measurement upper limit of B-type thermocouple, we fail to obtain the temperature at the lower region of HAB.

In Fig. 8, experimental temperature profiles of the ethanol spray flame are presented, where three

different zones in upper flame can be distinguished with the temperature varying. Ethanol sprays strongly burn accompanying a lot of exotherm under pure oxygen assistance, resulting in the formation of the high-temperature zone, in which the organometallic precursors tetrabutyl titanate will decompose, nucleate and grow to form condensed phase in the form of TiO_2 particles (solid or melting) due to its very low saturated vapor pressure (the local temperature almost within the range of the melting point (*ca.* 2150 K) and boiling point (*ca.* 3000 K) of TiO_2) [32]. Whereas Pt species are known to exist as gaseous PtO_2 under conditions of high temperature and oxidizing atmosphere [33]. This means that the two metal species separated and formed different states when undergoing the high temperature oxidation. Subsequently, a rapidly decaying on temperature in the quenching zone due to heat dissipation is provided by turbulent entrainment sheath gas. When temperature drops below 723 K [34], PtO_2 condenses from vapor to deposition phase in the form of isolated Pt atom dispersing on the surface of TiO_2 nanoparticles, consistent with the earlier AC–HAADF-STEM image (Fig. 5(b)) and XPS analysis about surface enrichment of Pt. However, a high Pt loading is conducive to growing into large Pt clusters over their dispersion, as observed in 0.5Pt/TiO_2 sample in Fig. 5(I). At the same time, the sheath gas Ar reduces temperature and the oxygen partial pressure in the flame downstream and makes the reversible reaction $PtO_2 \leftrightarrow Pt + O_2$ shift to the right. These different Pt-species vapors condense and deposit on TiO_2, forming Pt in different oxidation states shown in XPS analysis. Moreover, owing to the SMSI effect based on XPS and H_2-TPD analysis, the Pt atoms are anchored on TiO_2 to obtain very good stability. Eventually, it can yield an atomically dispersed catalyst at the low-temperature zone, as illustrated in insets of Fig. 8. The key to the whole synthesis process is summarized as high-temperature thermal separation and low-temperature surface deposition depending on temperature history.

4. Conclusions

Surface atomically dispersed Pt/TiO_2 catalysts are successfully synthesized by the FSP method that considers precursor choice and temperature history control, which exhibit extremely high activity and atom utilization for photocatalytic hydrogen production. Under ultra-low loading, Pt preferentially presents in the single-atomic oxidation state, which is the main active site for photocatalytic hydrogen evolution. For hydrogen production efficiency, the optimal Pt/TiO_2 catalyst with 0.1 mol% Pt greatly exceeds other reported Pt-loaded TiO_2 samples with similar content. This is a notable improvement for photocatalytic water splitting to hydrogen. FSP opens a door for synthesizing high-efficiency nanomaterials and has a great potential to reduce the high cost of noble metal catalysts. A feasible criteria of materials formulation aiming to produce surface single-atom catalysts, is the difference in the temperature onsets of species nucleation or condensation, generally relying on their saturated vapor pressure. In this work, based on the fact that the boiling point of TiO_2 is about 3000 K and the sublimation point of PtO_2 is about 723 K in an oxidizing atmosphere, it can be inferred that there is a tremendous difference in temperature ranges of the two species nucleation/condensation. Although precursors in solution are uniformly mixed on the atomic level at the start of FSP, an usual temperature history of "going up and then down" that is caused by combustion and quenching provides the process of high-temperature thermal separation and low-temperature surface deposition. Therefore, FSP offers a superior route in surface atomical engineering to tune the properties of supported catalysts.

Supplementary materials

Supplementary material associated with this article can be found, in the online version, at https://www.editorialmanager.com/PROCI/.

Declaration of Competing Interest

The authors declare that they have no known competing financial interests or personal relationships that could have appeared to influence the work reported in this paper.

Acknowledgments

This work was founded by National Natural Science Foundation of China (51920105009 and 51606079).

Supplementary materials

Supplementary material associated with this article can be found, in the online version, at doi:10.1016/j.proci.2020.06.330.

References

[1] K. Zeng, D. Zhang, *Prog. Energy Combust. Sci.* 36 (3) (2010) 307–326.
[2] T. Hisatomi, J. Kubota, K.J.C.S.R. Domen, *Chem. Soc. Rev.* 43 (22) (2014) 7520–7535.
[3] S. Chen, T. Takata, K. Domen, *Nat. Rev. Mater.* 2 (10) (2017) 17050.
[4] J.H. Montoya, L.C. Seitz, P. Chakthranont, A. Vojvodic, T.F. Jaramillo, J.K. Nørskov, *Nat. Mater.* 16 (1) (2016) 70–81.

[5] P. Roth, *Proc. Combust. Inst.* 31 (2) (2007) 1773–1788.
[6] S. Li, Y. Ren, P. Biswas, S.D. Tse, *Prog. Energy Combust. Sci.* 55 (2016) 1–59.
[7] G.A. Kelesidis, E. Goudeli, S.E. Pratsinis, *Proc. Combust. Inst.* 36 (1) (2017) 29–50.
[8] W.Y. Teoh, R. Amal, L. Mädler, *Nanoscale* 2 (8) (2010) 1324–1347.
[9] Y. Zhu, Z. Xu, K. Yan, H. Zhao, J. Zhang, *ACS Appl. Mater. Interfaces* 9 (46) (2017) 40452–40460.
[10] K.K. Akurati, A. Vital, G. Fortunato, R. Hany, F. Nueesch, T. Graule, *Solid State Sci.* 9 (3) (2007) 247–257.
[11] K. Nakata, A. Fujishima, *J. Photochem. Photobiol. C – Photochem. Rev.* 13 (3) (2012) 169–189.
[12] V. Etacheri, C. Di Valentin, J. Schneider, D. Bahnemann, S.C. Pillai, *J. Photochem. Photobiol. C – Photochem. Rev.* 25 (2015) 1–29.
[13] F. Yang, M. Liu, X. Chen, Z. Xu, H. Zhao, *Sol. RRL* 2 (12) (2018) 1800215.
[14] J. Yang, D. Wang, H. Han, C. Li, *Acc. Chem. Res.* 46 (8) (2013) 1900–1909.
[15] B. Qiao, A. Wang, X. Yang, L.F. Allard, Z. Jiang, Y. Cui, J. Liu, J. Li, T. Zhang, *Nat. Chem.* 3 (8) (2011) 634–641.
[16] J. Xing, J.F. Chen, Y.H. Li, W.T. Yuan, Y. Zhou, L.R. Zheng, H.F. Wang, P. Hu, Y. Wang, H.J. Zhao, Y. Wang, H.G. Yang, *Chem.-Eur. J.* 20 (8) (2014) 2138–2144.
[17] X. Li, W. Bi, L. Zhang, S. Tao, W. Chu, Q. Zhang, Y. Luo, C. Wu, Y. Xie, *Adv. Mater.* 28 (12) (2016) 2427–2431.
[18] A. Wang, J. Li, T. Zhang, *Nat. Rev. Chem.* 2 (6) (2018) 65–81.
[19] F. Niu, S. Li, Y. Zong, Q. Yao, *J. Phys. Chem. C* 118 (33) (2014) 19165–19171.
[20] K. Fujiwara, U. Müller, S.E. Pratsinis, *ACS Catal.* 6 (3) (2016) 1887–1893.
[21] K. Fujiwara, S.E. Pratsinis, *AIChE J.* 63 (1) (2017) 139–146.
[22] X. Chen, Z. Xu, F. Yang, H. Zhao, *Proc. Combust. Inst.* 37 (4) (2019) 5499–5506.
[23] I. Skenderovic, G. Kotalczyk, F.E. Kruis, *Processes* 6 (12) (2018) 253.
[24] J.E. Benson, M. Boudart, *J. Catal.* 4 (6) (1965) 704–710.
[25] Y.K. Kho, A. Iwase, W.Y. Teoh, L. Mädler, A. Kudo, R. Amal, *J. Phys. Chem. C* 114 (6) (2010) 2821–2829.
[26] J. Pan, G. Liu, G.Q. Lu, H.M. Cheng, *Angew. Chem., Int. Ed.* 50 (9) (2011) 2133–2137.
[27] C. Chaisuk, A. Wehatoranawee, S. Preampiyawat, S. Netiphat, A. Shotipruk, O. Mekasuwandumrong, *Ceram. Int.* 37 (5) (2011) 1459–1463.
[28] G. Xue-Qing, S. Annabella, D. Olga, J. Peter, D. Ulrike, *J. Am. Chem. Soc.* 130 (1) (2008) 370–381.
[29] M.C. Heine, L. Mädler, R. Jossen, S.E. Pratsinis, *Combust. Flame* 144 (4) (2006) 809–820.
[30] P.B. Neto, L. Buss, F. Meierhofer, H.F. Meier, U. Fritsching, D. Noriler, *Chem. Eng. Process.* 129 (2018) 17–27.
[31] C.S. McEnally, Ü.Ö. Köylü, L.D. Pfefferle, D.E. Rosner, *Combust. Flame* 109 (4) (1997) 701–720.
[32] Y. Kitamura, N. Okinaka, T. Shibayama, O.O.P. Mahaney, D. Kusano, B. Ohtani, T. Akiyama, *Powder Technol.* 176 (2) (2007) 93–98.
[33] C.B. Alcock, G.W. Hooper, R.S. Nyholm, *R. Soc. Lond. Proc.* 254 (1279) (1960) 551–561.
[34] J.C. Chaston, *Platinum Met. Rev.* 9 (1965) 51–56.